Atmos. Meas. Tech., 9, 2067–2076, 2016
www.atmos-meas-tech.net/9/2067/2016/
doi:10.5194/amt-9-2067-2016

Atmospheric Measurement Techniques
Open Access
EGU

MIPAS database: new HNO_3 line parameters at 7.6 µm validated with MIPAS satellite measurements

Agnès Perrin[1], Jean-Marie Flaud[1], Marco Ridolfi[2,3], Jean Vander Auwera[4], and Massimo Carlotti[5]

[1]Laboratoire Interuniversitaire des Systèmes Atmosphériques (LISA), UMR 7583 CNRS,
Universités Paris Est Créteil et Paris Diderot, Institut Pierre Simon Laplace, 61 avenue du Général de Gaulle,
94010 Créteil CEDEX, France
[2]Dipartimento di Fisica e Astronomia, Università di Bologna, 6/2 Viale Berti Pichat, 40127 Bologna, Italy
[3]Istituto di Fisica Applicata "N. Carrara" (IFAC) del Consiglio Nazionale delle Ricerche (CNR),
10 Via Madonna del Piano, 50019 Sesto Fiorentino (FI), Italy
[4]Service de Chimie Quantique et Photophysique, C.P. 160/09, Université Libre de Bruxelles,
50 avenue F.D. Roosevelt, 1050 Brussels, Belgium
[5]Dipartimento di Chimica Industriale "Toso Montanari", Università di Bologna,
4 Viale del Risørgimento, 40136 Bologna, Italy

Correspondence to: Agnès Perrin (agnes.perrin@lisa.u-pec.fr)

Received: 23 September 2015 – Published in Atmos. Meas. Tech. Discuss.: 10 November 2015
Revised: 25 March 2016 – Accepted: 6 April 2016 – Published: 10 May 2016

Abstract. Improved line positions and intensities have been generated for the 7.6 µm spectral region of nitric acid. They were obtained relying on a recent reinvestigation of the nitric acid band system at 7.6 µm and comparisons of HNO_3 volume mixing ratio profiles retrieved from the Michelson Interferometer for Passive Atmospheric Sounding (MIPAS) limb emission radiances in the 11 and 7.6 µm domains. This has led to an improved database called MIPAS-2015. Comparisons with available laboratory information (individual line intensities, integrated absorption cross sections, and absorption cross sections) show that MIPAS-2015 provides an improved description of the 7.6 µm region of nitric acid. This study should help to improve HNO_3 satellite retrievals by allowing measurements to be performed simultaneously in the 11 and 7.6 µm micro-windows. In particular, it should be useful to analyze existing MIPAS and IASI spectra as well as spectra to be recorded by the forthcoming Infrared Atmospheric Sounding Interferometer – New Generation (IASI-NG) instrument.

1 Introduction

Optical remote sensing of nitric acid in the infrared range can be performed using the three strongest band systems of this species, namely the $\{\nu_5, 2\nu_9\}$, $\{\nu_3, \nu_4\}$, and ν_2 band systems located near 11, 7.6, and 5.8 µm respectively. Focusing on the spectral ranges covered by the Michelson Interferometer for Passive Atmospheric Sounding (MIPAS) instrument (Fischer et al., 2008) that was operational on board the ENVISAT satellite (Endemann, 1999) in the years from 2002 to 2012, Flaud et al. (2006 and references therein) created a HNO_3 linelist covering the 600–1800 cm^{-1} region with the aim to provide the best and most consistent possible set of line parameters (positions, intensities, and shape-specific parameters) for this molecular species. Subsequent laboratory and theoretical studies (Gomez et al., 2009; Laraia et al., 2009) revisited this linelist. The updated linelist thus produced and validated (Tran et al., 2009) is implemented in the HITRAN (Rothman et al., 2009, 2013) and GEISA (Jacquinet-Husson et al., 2011) databases. It will be called MIPAS-OLD in the following.

The integrated absorption cross sections of the 11, 7.6, and 5.8 µm regions are in the ratios $I(11\,\mu m)/I(7.6\,\mu m)/I(5.8\,\mu m) = 1.00/2.1/2.4$ (Chackerian et al., 2003). Although 2 times weaker than the bands

observed in the two other ranges, the 11 µm band system is however of particular atmospheric interest since (i) it coincides with a rather clear atmospheric window and (ii) the corresponding line parameters are of good quality. At 11 µm, the MIPAS-OLD linelist indeed includes not only the ν_5 and $2\nu_9$ cold bands for the $H^{14}N^{16}O_3$ and $H^{15}N^{16}O_3$ isotopic species (see Perrin et al., 2004, 2006 and references therein), but also the $\nu_5+\nu_9-\nu_9$, $3\nu_9-\nu_9$, $\nu_5+\nu_7-\nu_7$, and $\nu_5+\nu_6-\nu_6$ hot bands of $H^{14}N^{16}O_3$ (Flaud et al., 2003; Mencaraglia et al., 2006; Gomez et al., 2009). The line broadening coefficients were calculated using a semi-classical approach (Gomez et al., 2009; Laraia et al., 2009). The MIPAS-OLD database then provides an excellent description of the nitric acid spectrum at 11 µm (Tran et al., 2009), and is used for HNO_3 retrievals by numerous satellite or balloon-borne instruments (Irie et al., 2006; Raspollini et al., 2006, 2013; Wang et al., 2007; Wolff et al., 2008; Wespres et al., 2009).

However, retrievals of nitric acid at altitudes higher than $\sim$ 35–40 km would benefit from the use of the stronger infrared signatures at 5.8 or 7.6 µm. A thorough error analysis shows that, since the first spectral region overlaps rather strongly with water vapor absorption in atmospheric spectra, it is preferable to use the 7.6 µm band system. However, the quality of retrievals in this spectral range was up to now hampered by the rather poor quality of the HNO_3 line positions and line intensities.

The present effort aims to provide for the 7.6 µm spectral region of nitric acid spectroscopic data of the best possible quality in order to allow the retrieval of this species using the 11 and 7.6 µm regions simultaneously. It relies on an improved analysis of the nitric acid band system at 7.6 µm (Perrin, 2013), summarized in Sect. 2, and comparisons of HNO_3 volume mixing ratio (VMR) profiles retrieved from MIPAS limb emission radiances using MIPAS-OLD line parameters for the 11 µm region and the updated spectroscopic information generated in the present work for the 7.6 µm range. This work is described in Sect. 3. The resulting linelist, called MIPAS-2015, thus contains new and more precise information for the 7.6 µm region of HNO_3, as compared to MIPAS-OLD. The quality of the update was evaluated by comparisons with available laboratory information (individual line intensities, integrated absorption cross sections, and absorption cross sections). This assessment of the MIPAS-2015 linelist is described in Sect. 4.

2 Improved analysis of the 7.6 µm region of HNO_3

At 7.6 µm, the MIPAS-OLD data originate from two laboratory studies, focused on line positions (Perrin et al., 1989) and line intensities (Perrin et al., 1993). The corresponding linelist is limited to the ν_3 and ν_4 bands of the main isotopologue, $H^{14}N^{16}O_3$, and the quality of the corresponding line positions and intensities is rather poor. Indeed, the theoretical model used to calculate the upper state energy levels accounted only for resonances coupling energy levels belonging to the V3 and V4 bright states, neglecting contributions from several dark states present in the same energy range (see Table 1), thus limiting the quality of the frequency analysis (Perrin et al., 1989). The subsequent updates (Godman et al., 1998; Flaud et al., 2006), which consisted only in an absolute intensity calibration, did not improve the situation.

A complete reinvestigation of the ν_3 and ν_4 bands of nitric acid at 7.6 µm was performed recently (Perrin, 2013). Contrary to the previous analysis (Perrin et al., 1989, 1993, 1989), the new Hamiltonian model accounts fully for the various vibration–rotation resonances and torsional effects affecting the V3 and V4 bright states and the four dark states 2V6, 3V9, V5 + V9, and V7 + V8. The relative line intensities at 7.6 µm were calculated, also accounting for the observed resonances (Perrin, 2013). Additionally, the $\nu_3+\nu_9-\nu_9$ hot band could be identified for the first time (Perrin, 2013).

3 The MIPAS-2015 linelist with intensities at 7.6 µm calibrated using HNO_3 retrievals from MIPAS radiances at 11 and 7.6 µm

Following the work of Perrin (2013), we have generated a list of line positions and relative line intensities for the 7.6 µm region of the spectrum of nitric acid. It includes (see Table 1) the ν_3 and ν_4 cold bright bands, the $2\nu_6$, $3\nu_9$, $\nu_5+\nu_9$, $\nu_7+\nu_8$ cold weak bands, and the $\nu_3+\nu_9-\nu_9$ hot band of the main isotopologue. Line shape parameters (air- and self-broadening coefficients, temperature dependence of the air-broadening coefficient, and air-shift coefficients) were added using the corresponding information available in MIPAS-OLD for the 11 µm spectral range of HNO_3 (Rothman et al., 2009). The HNO_3 linelist at 7.6 µm of the MIPAS-OLD database was completely replaced by the new linelist, leading to the so-called MIPAS-2015 linelist. The remainder of MIPAS-OLD was left unchanged.

Using MIPAS radiances, an absolute intensity calibration was performed to "convert" the relative line intensities at 7.6 µm to absolute intensities. More precisely, this was done by comparing HNO_3 VMR retrieved from MIPAS radiances using the MIPAS-2015 linelist in either the 7.6 or the 11 µm regions. A multiplicative factor was applied to all the line intensities at 7.6 µm so that in the height range of the HNO_3 VMR peak ($\sim$ 21–24 km), the VMR retrieved using the 7.6 µm interval matches that retrieved using the 11 µm region.

The retrieval algorithm used for the tests presented in this work is the so-called optimized retrieval model (ORM) version 7.0, that is, the scientific prototype of the code used by the European Space Agency (ESA) for routine MIPAS data processing (Ridolfi et al., 2000; Raspollini et al., 2006, 2013). The retrieval is based on the inversion of narrow (max $3\,cm^{-1}$) spectral intervals, called micro-windows (MWs). The MWs used in our test retrievals are listed in Table 2. These are selected using the MWMAKE algorithm of Dudhia et al. (2002). Out of a user-supplied broad spectral inter-

Table 1. HNO_3 vibrational states involved in the 7.6 µm region.

Band	Type[a]	Upper[b] vibration[b]	Lower vibration[b]	Upper state (cm^{-1}) (deperturbed value)[c]	Lower state (cm^{-1})	Band center[c] (cm^{-1})
ν_3	bright	V3	GROUND	1326.186	0	1326.186
ν_4	bright	V4	GROUND	1303.073	0	1303.073
$2\nu_6$	dark	2V6	GROUND	1289.466	0	1289.466
$\nu_5+\nu_9$	dark	V5 + V9	GROUND	1339.47	0	1343.78
$\nu_7+\nu_8$	dark	V7 + V8	GROUND	1341.063	0	1341.063
$3\nu_9$	dark	3V9	GROUND	1293.186	0	1288.899
$\nu_3+\nu_9-\nu_9$	bright	V3 + V9	V9	1789.317	458.229	1331.088

[a] Type: bright and dark indicate observed and non-observed transitions, respectively.
[b] Upper and lower vibrations: vibration states of HNO_3 as coded in the MIPAS, HITRAN (Rothman et al., 2013), and GEISA (Jacquinet-Husson et al., 2011) databases.
[c] See Perrin (2013) for details.

Table 2. Micro-windows used for HNO_3 retrievals at 11 and 7.6 µm.

11 µm			7.6 µm region		
Channel	σ_{min}	σ_{max}	Channel	σ_{min}	σ_{max}
HNO30507	863.4750	866.4750	HNO30514	1309.150	1312.150
HNO30503	866.5000	869.5000	HNO30511	1313.725	1316.725
HNO30508	869.5250	872.5250	HNO30515	1316.850	1319.850
HNO30502	878.4250	881.4250	HNO30513	1324.200	1327.200
HNO30501	885.0000	888.0000	HNO30516	1329.375	1332.375
HNO30506	888.0250	891.0250	HNO30512	1333.525	1336.525

Channel is a MIPAS identifier; σ_{min} and σ_{max} (cm^{-1}) are the lower and higher wavenumber limits of the micro-windows.

val, this algorithm selects optimized MWs that contain relevant information on the atmospheric target parameters to be retrieved (the HNO_3 VMR in our case). The selection aims at the minimization of the total retrieval error. The latter is evaluated, taking into account the measurement noise, the errors due to the uncertainties in the (previously retrieved) pressure and temperature, the error due to spectral interferences of non-retrieved atmospheric gases, and several instrument and forward model errors. The full list of the considered error components is reported in Dudhia (2007). In order to limit the influence of the error due to the mutual spectral interference of the main atmospheric emitting gases, in the test retrievals presented in this study we adopt the following retrieval strategy: first we jointly retrieve tangent pressures and the temperature profile then, sequentially, we retrieve the VMR profiles of H_2O, O_3, HNO_3, CH_4, N_2O, and NO_2. For the remaining interfering gases we assume the climatological profiles of Remedios et al. (2007).

At the end of the MW selection process, MWMAKE provides estimates of the various error components affecting the HNO_3 VMR profile derived from the inversion of the selected MWs. As an example, at 21 km height, for the MWs listed in Table 2 we get following error estimates.

a. When using the MWs at 11 µm we get the total error due to the uncertainties in pressure, temperature, and its horizontal gradient, 4 %. The interference error due to H_2O is 0.2 %; the interference error due to NH_3 is < 0.1 %. The error due to radiometric and instrument line shape (ILS) calibration is 2 %. Other error sources are much smaller than the above contributions.

b. When using the MWs at 7.6 µm we get the total error due to the uncertainties in pressure, temperature, and its horizontal gradient, 14 %. The interference error due to H_2O is 6.7 %; the interference error due to N_2O is 2.3 %; the interference error due to CH_4 is 3.4 %; The error due to radiometric and ILS calibration is 2 %. Other error sources are much smaller than the above contributions.

MWMAKE also provides an estimate of the error due to measurement noise; however, being based on *assumed* instrument radiometric performance figures, the estimate itself is not extremely accurate. A more reliable estimate of this error is provided by the covariance matrix of the Levenberg–Marquardt inversion method (Ceccherini et al., 2010), that is, based on the actual noise determined by the MIPAS Level 1b

processor for each measurement. At the altitude of 21 km this method provides, on average, an error of 1.8 % when using the MWs at 11 µm, and of 2.4 % when using the MWs at 7.6 µm. Note that apart from the error due to radiometric and ILS calibration, all the other error components mentioned above behave randomly when considering a statistically significant set of retrieved profiles spanning the whole globe.

The left panel of Fig. 1 shows averages of 929 HNO_3 VMR profiles retrieved from the MIPAS limb scanning radiances (Level 1b version 7.11) acquired on 24 January 2003 with a Fourier transform spectrometer spectral resolution of 0.025 cm^{-1}. In this test, the profiles are retrieved using the MIPAS-2015 linelist and MWs, alternately in the 11 µm region (red line) or in the 7.6 µm region (blue line). Being the average of a large number of profiles, the noise error bars are not visible in the plot. We notice that the profiles retrieved from the two spectral regions are in excellent agreement. To better quantify the residual discrepancies, in the right panel of Fig. 1 we show the percentage differences (black line) between the average profiles retrieved using MWs in the 7.6 and in the 11 µm region. The error bars of the black line represent the statistical error of the mean difference. At each altitude, this error is calculated as the standard deviation of the profile differences divided by the square root of the number of samples at the considered altitude. It accounts, therefore, for all the components of the VMR error that, as mentioned above, vary randomly within our sample. Note that, especially in the altitude range from 15 to 30 km, where the individual profile retrievals are more stable due to the larger sensitivity of the limb measurements to the HNO_3 amount, the maximum bias between the average profiles is less than 0.8 %. Being the average of a large number of profiles, the random error on the evaluated bias (error bars of the black line of Fig. 1) is rather small.

An additional (systematic) error on the evaluated bias arises from the inter-band radiometric calibration error in the MIPAS spectra used (Kleinert et al., 2007). The radiometric calibration of MIPAS spectra is constant within the set of measurements considered in the tests of Fig. 1. However, since it is renewed on a weekly basis, to evaluate the impact of this error source in the calibration of the HNO_3 linelist in the 7.6 µm region, we repeated the test illustrated in Fig. 1 with different sets of MIPAS measurements with different radiometric calibrations. We selected MIPAS measurements acquired in three different days of the years 2002 and 2003 (still measurements acquired with the MIPAS full spectral resolution of 0.025 cm^{-1}). The results of these additional tests show that, actually, the observed differences between the average HNO_3 VMR retrieved from the 11 and the 7.6 µm regions amount to a maximum of 1.5 % in the height range from 15 to 30 km. This is the accuracy we attribute to our HNO_3 linelist calibration procedure. The blue and red lines in the right panel of Fig. 1 indicate the ± noise error of an individual profile retrieval determined from the covariance matrix of the Levenberg–Marquardt inversion method

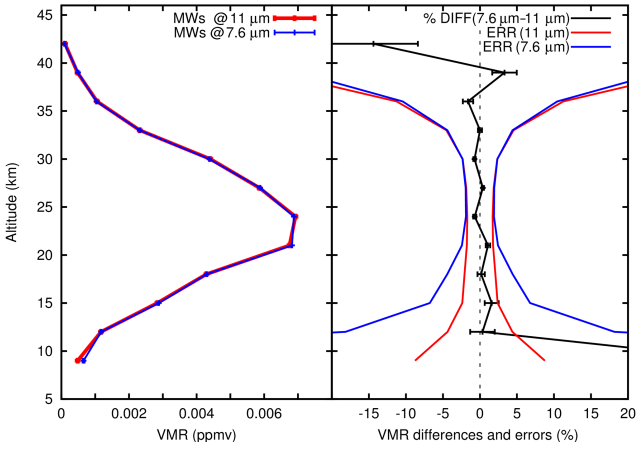

Figure 1. Left panel: average HNO_3 VMR profiles from MIPAS measurements acquired on 24 January 2003, using the MIPAS-2015 linelist. Retrievals using MWs in the 11 µm region (red line) and in the 7.6 µm region (blue line). Right panel: mean percentage differences between HNO_3 profiles retrieved from the 7.6 and 11 µm regions (black line). The red and the blue lines show the noise error of the individual retrievals using MWs in the 11 and in the 7.6 µm spectral regions.

(Ceccherini et al., 2010). While the inversion with the MWs in the 11 µm region provides a smaller retrieval error below 23 km, the MWs in the 7.6 µm region provide a smaller error above 30 km. This behavior is due to the larger intensity of the HNO_3 band system in the 7.6 µm region. This effect is however noticeable only at high altitudes. In the troposphere or lower stratosphere the presence of H_2O emission lines in the 7.6 µm region masks the signal from HNO_3.

As a term of comparison, to better highlight the achieved improvements, in Fig. 2 we show the results of a test analogous to that of Fig. 1, but using the MIPAS-OLD line database. We see that in this case the agreement between the HNO_3 VMR retrieved from the 11 and 7.6 µm regions is not better than 8–10 %.

Beyond the better consistency between the two HNO_3 band systems at 11 and 7.6 µm, the new HNO_3 linelist at 7.6 µm allows a much more accurate simulation of the MIPAS-observed spectra. The average normalized chi-square value of the inversion fit with the MWs selected in the 7.6 µm region changes from the value of 1.616 achieved with the MIPAS-OLD linelist, to the value of 1.227 with the MIPAS-2015 linelist. This reduction in the chi-square value is clearly due to the improvement of the residuals of the fit, i.e., of the differences between observed and simulated spectra. To show the improvements in the residuals, for the MIPAS orbit 04712 acquired on 24 January 2003, we computed the average observed spectrum, the average simulated spectrum, and the average residual spectrum for the two test retrievals using the MIPAS-OLD and the MIPAS-2015 HNO_3 linelists. We obtained the average by co-adding the spectra

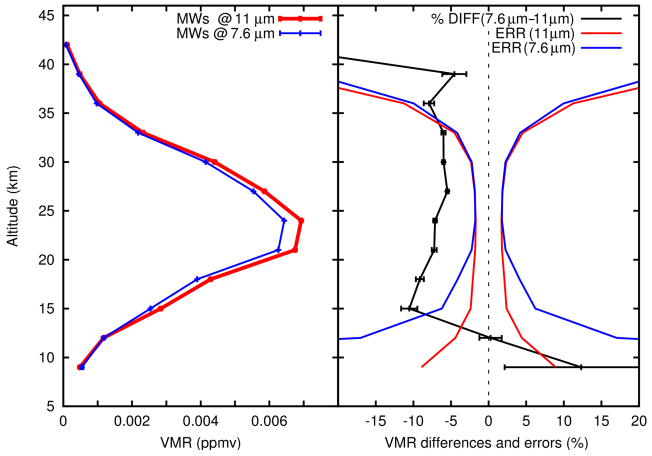

Figure 2. Left panel: average HNO_3 VMR profiles from MIPAS measurements acquired on 24 January 2003, using the MIPAS-OLD linelist. Retrievals using MWs in the 11 µm region (red line) and in the 7.6 µm region (blue line). Right panel: mean percentage differences between HNO_3 profiles retrieved from the 7.6 and 11 µm regions (black line). The red and the blue lines show the noise error of the individual retrievals using MWs in the 11 and in the 7.6 µm spectral regions.

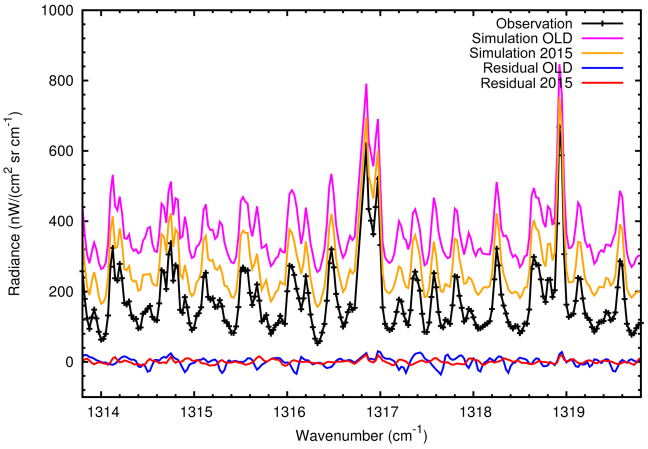

Figure 3. Average MIPAS-observed spectrum (black) in the 1314–1320 cm^{-1} spectral region, and spectra simulated with the MIPAS-OLD (magenta line) and the MIPAS-2015 (orange line) HNO_3 linelists. For better readability of the plot, the average orange and magenta lines were shifted by 100 and 200 nW $(cm^2\,sr\,cm^{-1})^{-1}$ respectively. The blue and the red lines are the residuals obtained with the MIPAS-OLD and the MIPAS-2015 linelists respectively.

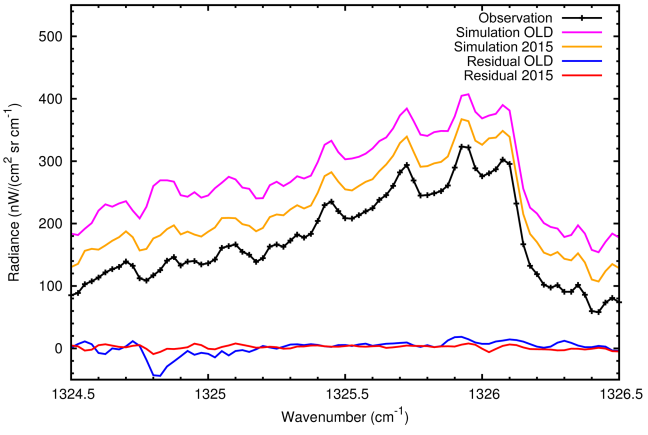

Figure 4. Average MIPAS-observed spectrum (black) in the 1324.5–1326.5 cm^{-1} spectral region, and simulated spectra with the MIPAS-OLD (magenta line) and the MIPAS-2015 (orange line) HNO_3 linelists. For better readability of the plot, the average orange and magenta lines were shifted by 50 and 100 nW $(cm^2\,sr\,cm^{-1})^{-1}$ respectively. The blue and the red lines are the residuals obtained with the MIPAS-OLD and the MIPAS-2015 linelists respectively.

with nominal tangent altitudes of 21, 24, 27, and 30 km. In total, each average spectrum is the result of a co-adding of 288 individual spectra. Since MIPAS measurement noise in the 7.6 µm region is of the order of 14 nW $(cm^2\,sr\,cm^{-1})^{-1}$, the noise error on the average residuals is of the order of 0.8 nW $(cm^2\,sr\,cm^{-1})^{-1}$, i.e., much smaller than the actual features observed in the residuals themselves.

In Figs. 3–5 we show some average spectra and residuals. In each of these figures the black line is the average observed spectrum; the magenta and orange lines are the average simulations obtained with the MIPAS-OLD and the MIPAS-2015 linelists respectively. For better readability of the plots, the lines representing the average simulated spectra are shifted with respect to the observation as specified in the figure caption. The blue and the red lines represent the average residuals computed as the difference between the average observation and the average simulation using, respectively, the MIPAS-OLD and the MIPAS-2015 HNO_3 linelists. From these figures we can clearly appreciate improvements in the residual spectra achieved with the new HNO_3 linelist. In fact such improvements are due, on the one hand to the fact that thanks to an improved theoretical model which accounts for the resonance effects, the cold bands are much better modeled, and on the other hand to the inclusion of the hot band $\nu_3 + \nu_9 - \nu_9$ (see Table 3 and Fig. 5). More precisely, Table 3 compares the information available for the 7.6 µm region of HNO_3 in the MIPAS-OLD and MIPAS-2015 databases. It shows that the new database includes lines from four weak bands ($2\nu_6$, $\nu_5+\nu_9$, $\nu_7+\nu_8$ and $3\nu_9$) together with those from the ν_3 and ν_4 bands which were already present in MIPAS-OLD: this is because the theoretical model used in 2013 (Perrin, 2013) to generate the linelist is more sophisticated than in 1993 (Perrin et al., 1993).

Table 3. HNO_3 line parameters in the 7.6 µm region.

(a) The MIPAS-OLD database						
Band	NB	S_{tot} (10^{-18})	σ_{min}	σ_{max}	S_{min} (10^{-23})	S_{max} (10^{-21})
ν_3	21 308	25.37	1098.376	1387.849	1.037	31.33
ν_4	19 584	12.78	1229.867	1387.561	1.037	18.67
Sum		38.15				
(b) The MIPAS-2015 database						
Band	NB	S_{tot} (10^{-18})	σ_{min}	σ_{max}	S_{min} (10^{-25})	S_{max} (10^{-21})
ν_3	16 408	24.940	1252.010	1394.177	4.910	32.0
ν_4	18 105	9.834	1238.929	1387.081	4.020	21.4
$2\nu_6$	2451	0.119	1243.465	1348.275	4.624	3.660
$\nu_5 + \nu_9$	13 817	0.716	1246.929	1390.071	2.081	3.543
$\nu_7 + \nu_8$	11 125	0.761	1246.422	1395.679	2.314	5.017
$3\nu_9$	13 894	1.177	1233.107	1388.497	4.582	2.378
Sum		37.547				
$\nu_3 + \nu_9 - \nu_9$	12 106	1.408	1271.050	1394.899	5.285	1.798

NB is the number of lines; σ_{min} and σ_{max} (cm^{-1}) give the wavenumber range of the bands; S_{min} and S_{max} are the smallest and largest line intensity in cm^{-1} (molecule $cm^2)^{-1}$ at 296 K; S_{tot} is the sum of the line intensities in cm^{-1} (molecule $cm^2)^{-1}$ at 296 K.

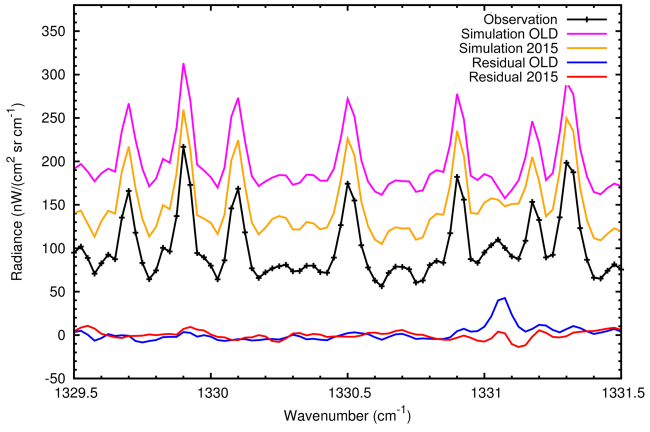

Figure 5. Average MIPAS-observed spectrum (black) in the 1329.5–1331.5 cm^{-1} spectral region, and simulated spectra with the MIPAS-OLD (magenta line) and the MIPAS-2015 (orange line) HNO_3 linelists. For better readability of the plot, the average orange and magenta lines were shifted by 50 and 100 nW $(cm^2\,sr\,cm^{-1})^{-1}$ respectively. The blue and the red lines are the residuals obtained with the MIPAS-OLD and the MIPAS-2015 linelists respectively.

4 Assessment of the MIPAS-2015 linelist

This chapter is devoted to the comparison of the MIPAS-2015 linelist with the experimental data available in the literature. They can consist in individual intensities measured at high resolution, or integrated band intensities or absorption cross sections measured at medium or low resolution.

4.1 Individual line intensities at 7.6 µm

To the best of our knowledge, individual line intensities have been measured in the 7.6 µm region of the HNO_3 spectrum in only two contributions (May and Webster, 1989; Perrin et al., 1993). Laboratory measurements of individual line intensities are indeed rather difficult for HNO_3 since the line widths ($\gamma_{Voigt} \sim 0.002\,cm^{-1}$ in laboratory conditions usually used for this unstable species (296 K and 0.3 hPa)) are of the same order of magnitude as the separation of adjacent lines (from 0.002 to 0.010 cm^{-1}), resulting in a lot of blended lines. Intensities measured for blended lines being most probably characterized by a reduced precision, the comparison between line intensities reported in these two studies and those included in the MIPAS-2015 database was limited to well-identified and unblended lines. Table 4 presents the averages of the ratios $R = \text{Int(MIPAS-2015)} / \text{Int(Obs)}$ of line intensities in MIPAS-2015 with the corresponding measured values. It shows that, on average, the line intensities of MIPAS-2015 are about 27 % weaker and 39 % stronger than measured by May and Webster (1989) and Perrin et al. (1993), respectively.

In view of these diverging results, we decided to measure individual line intensities for nitric acid using a Fourier transform spectrum, recorded in Giessen in 2002 (Perrin

Table 4. Average ratios R_{mean} of line intensities included in MIPAS-2015 (at 296 K) and measured in the literature and in this work.

Report	No.	R_{mean}
May and Webster (1989) (296 K)	256	0.73 (21)
Perrin et al. (1993) (271 K)	40	1.39 (21)
This work (299.7 K)	348	0.95 (18)

The comparison accounts for the temperature conversion to 296 K; no. is the number of line intensities included in the average. The numbers in parentheses are the standard deviations, in the units of the last digit quoted.

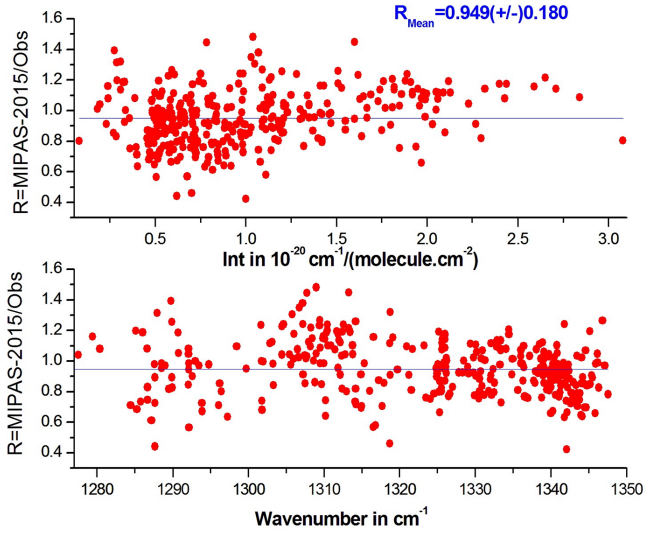

Figure 6. Comparison between the line intensities measured in this work using a Fourier transform spectrum (Obs, 299.7 K, 0.03 hPa, absorption path length = 302 cm, Perrin et al., 2004; Perrin, 2013) and those available in MIPAS-2015. The comparison, performed as a function of the intensities and wavenumbers (upper and lower panels, respectively), accounts for the temperature correction from 299.7 to 296 K.

et al., 2004). This spectrum was recorded in the 718–1436 cm^{-1} spectral region at 299.7 K, at a pressure of 0.03 hPa and with an absorption path length of 302 cm (more details can be found in Perrin et al., 2004). Assuming a Gaussian line profile and including instrumental effects arising from the maximum optical path difference of 542 cm and the 1.3 mm entrance aperture used, 348 line intensities were measured for well-isolated lines in the 7.6 µm region using the program WSpectra (Carleer et al., 2001). Figure 6 presents an overview of the comparison between these measured line intensities and those available in MIPAS-2015.

No clear trend with respect to line positions or line intensities is noticeable. On average, the intensities quoted in MIPAS-2015 are only 5 % smaller than those measured during the present investigation. As shown in Table 4, this corresponds to a much better agreement than with previous works, although this is not a definite confirmation of the accuracy of the line intensities in MIPAS-2015 because the uncertainty of measurement of the HNO_3 pressure for the Giessen spectrum is not precisely known. It is worth noting that large variations of the ratio R are observed, as shown in Fig. 6; they reflect in the standard deviation on R which is rather large. Similar behaviors were observed for the other two sets of line by line intensity measurements (May and Webster, 1989; Perrin et al., 1993). Possible explanations of these rather large standard deviations include the fact that it is not always possible to avoid blended lines in the congested 7.6 µm spectral region, even if care was taken to avoid them, and that the theoretical model used to compute the line intensities is still imperfect, as discussed in detail in Perrin (2013).

4.2 Integrated band intensities

Flaud et al. (2006) reviewed the integrated band intensities reported in the literature at 11 and 7.6 µm (Goldman et al., 1971; Giver et al., 1984; Massie et al., 1985; Hjorth et al., 1987; Chackerian et al., 2003). As shown in Table 5, these literature results are in reasonable agreement with each other.

As measured integrated band intensities include the contributions of hot bands and bands from isotopologues other than $H^{14}N^{16}O_3$, comparison of the experimental integrated band intensities with the sum of the individual line intensities listed in the MIPAS databases require use of the following expression (see Appendix A of Flaud et al., 2006 and Rotger et al., 2008):

$$S_{band}(T) \approx \frac{Z_{vib}(T)}{I_a} \sum_k S_k, \quad (1)$$

where S_k is the intensity of line k in the MIPAS database accounting for the isotopic abundance, $Z_{vib}(T)$ is the vibrational partition function of $H^{14}N^{16}O_3$ (Z_{vib} (296 K) = 1.29952) and $I_a = 0.989$ is its isotopic abundance. The summation in Eq. (1) runs over all the lines of all the cold bands listed in Table 3. In Table 5, the integrated band intensities calculated using MIPAS-OLD and MIPAS-2015 with Eq. (1) are compared with the experimental values reported for the 11 and 7.6 µm regions. Considering their associated uncertainties, one can say that MIPAS-2015 is in agreement with the most recent measurements.

4.3 Absorption cross sections

We also performed direct comparisons with the experimental absorption cross sections available in the Pacific Northwest National Laboratory (PNNL) library (Sharpe et al., 2004).

Figure 7 compares the PNNL experimental absorption cross sections at 7.6 µm with absorption cross sections calculated at the same conditions using MIPAS-2015 and MIPAS-OLD (assuming that the N_2-broadening coefficients are the same as the air-broadening coefficients provided in these databases). Figure 7 shows that the agreement is significantly

Table 5. Comparison of measured and calculated HNO_3 integrated band intensities in the 11 µm (820–950 cm^{-1}) and 7.6 µm (1240–1400 cm^{-1}) spectral ranges.

Reference	$^{11\,\mu m}S_{band}$ (296 K)	$^{7.6\,\mu m}S_{band}$ (296 K)	$^{7.6\,\mu m/11\,\mu m}R$
Goldman et al. (1971)	2.39 (37)	4.66 (40)	1.95 (47)
Giver et al. (1984)	2.57 (13)	5.15 (16)	2.00 (16)
Massie et al. (1985)	1.98 (30)	3.72 (56)	1.88 (57)
Hjorth et al. (1987)	2.21 (33)	4.29 (60)	1.94 (78)
Chackerian et al. (2003)	2.424 (65)	5.09 (18)	2.10 (13)
PNNL[1], Sharpe et al. (2004)	2.538 (85)	5.04 (17)	1.99 (13)
MIPAS-OLD[2] Flaud et al. (2006)	2.335	5.013	2.148
MIPAS-2015[2] (This work)	2.335	4.934	2.109

All the intensities are given in 10^{-17} cm^{-1} (molecule $cm^2)^{-1}$ at $T = 296$ K,
$^{7.6\,\mu m/11\,\mu m}R = {}^{7.6\,\mu m}S_{band}(296\,K)/{}^{11\,\mu m}S_{band}(296\,K)$.
[1] PNNL: Pacific Northwest National Laboratory.
[2] To estimate the integrated band intensities for MIPAS-OLD and MIPAS-2015, the sums of the cold band intensities (listed in Table 3) are multiplied by 1.314 (see text for details).

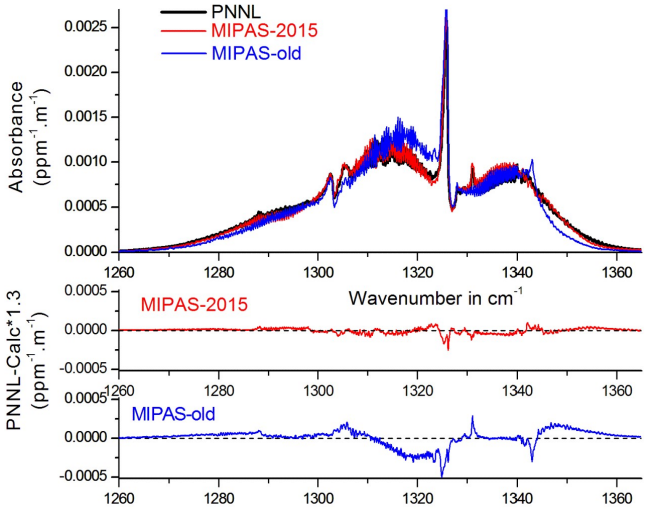

Figure 7. Upper panel: absorption cross sections from PNNL (Sharpe et al., 2004, black trace), and calculated using MIPAS-OLD (blue trace) and MIPAS-2015 (red trace); lower panel: corresponding residuals. For these calculations, the contributions of hot bands and bands from isotopologues other than $H^{14}N^{16}O_3$ were accounted for by multiplying the calculated absorption cross sections by the ratio $Z_{Vib}(300\,K)/I_a = 1.314$ (see Eq. 1).

better with MIPAS-2015. In particular, the improvement is really significant at 1331.1, 1341.1, and 1343.8 cm^{-1}; this is because the contribution of the $\nu_3 + \nu_9 - \nu_9$ hot band and of the $\nu_7 + \nu_8$ and $\nu_5 + \nu_9$ dark bands are correctly accounted for in the new database.

5 Conclusions

An improved set of line positions and intensities called MIPAS-2015 has been generated for the 7.6 µm spectral region of nitric acid. They were obtained relying on a recent reinvestigation of the nitric acid band system at 7.6 µm and on comparisons of HNO_3 volume mixing ratio profiles retrieved from the MIPAS limb emission radiances in the 11 and 7.6 µm domains. Comparisons with available laboratory information (individual line intensities, integrated absorption cross sections, and absorption cross sections) showed the improvement brought by the new database MIPAS-2015 as compared to the old one clearly.

Data availability

The HNO_3 line parameters included in the MIPAS-2015 linelist can be downloaded from http://atmos.difa.unibo.it/spectdb/hno3_mipas_2015_4.45.par.zip. Scientists using the data are kindly invited to cite the present paper in the publications that may arise from their research work.

Acknowledgements. Validation studies involving MIPAS measurements are supported by the ESA ESRIN contract no. 4000112093/14/LG. Financial support from the CNRS-INSU (Institut National des Sciences de l'Univers) of the CNRS through the Les enveloppes fluides et l'Environnement de Chimie Atmosphèrique (LEFE-CHAT) program, and from the CNES (Centre National de la Recherche Spatiale, France) through the project IASI-TOSCA are acknowledged. Part of this work was also supported by the GDRIHiResMir (Groupement de Recherche International HiResMir High resolution microwave, infrared and Raman molecular spectroscopy for atmospheric, planetological and astrophysical applications). J. Vander Auwera is senior research associate with the F.R.S.-FNRS.

Edited by: J. Notholt

References

Carleer, M. R.: WSpectra: a Windows program to accurately measure the line intensities of high-resolution Fourier transform spectra, in: Remote Sensing of Clouds and the Atmosphere V, edited by: Russel, J. E., Schäfer, K., and Lado-Bordowsky, O., Proceedings of SPIE – The International Society for Optical Engineering, 4168, Barcelona, Spain, 337–342, 2001.

Ceccherini, S. and Ridolfi, M.: Technical Note: Variance-covariance matrix and averaging kernels for the Levenberg-Marquardt solution of the retrieval of atmospheric vertical profiles, Atmos. Chem. Phys., 10, 3131–3139, doi:10.5194/acp-10-3131-2010, 2010.

Chackerian, C., Sharpe, S. W., and Blake, T. A.: Anhydrous nitric acid integrated absorption cross sections: 820–5300 cm^{-1}, J. Quant. Spectrosc. Ra., 81, 429–441, 2003.

Dudhia, A.: MIPAS Microwindow error analysis, available at: www.atm.ox.ac.uk/group/mipas/err/ (last access: 21 March 2016), 2007.

Dudhia, A., Jay, V. L., and Rodgers, C. D.: Microwindow selection for high-spectral-resolution sounders, Appl. Optics, 41, 3665–3673, 2002.

Endemann, M.: MIPAS instrument concept and performance, in: Proceedings of the ESAMS'99, 18–22 January 1999, Noordwijk, the Netherlands, ESTEC-ESA, WPP-161, 1, 29–43, ISSN: 1022-6656, 1999.

Fischer, H., Birk, M., Blom, C., Carli, B., Carlotti, M., von Clarmann, T., Delbouille, L., Dudhia, A., Ehhalt, D., Endemann, M., Flaud, J. M., Gessner, R., Kleinert, A., Koopman, R., Langen, J., López-Puertas, M., Mosner, P., Nett, H., Oelhaf, H., Perron, G., Remedios, J., Ridolfi, M., Stiller, G., and Zander, R.: MIPAS: an instrument for atmospheric and climate research, Atmos. Chem. Phys., 8, 2151–2188, doi:10.5194/acp-8-2151-2008, 2008.

Flaud, J.-M., Perrin, A., Orphal, J., Kou, Q., Flaud, P.-M., Dutkiewicz, Z., and Piccolo, C.: New analysis of the $\nu_5 + \nu_9$-ν_9 hot band of HNO_3, J. Quant. Spectrosc. Ra., 77, 355–364, 2003.

Flaud, J.-M., Brizzi, G., Carlotti, M., Perrin, A., and Ridolfi, M.: MIPAS database: Validation of HNO3 line parameters using MIPAS satellite measurements, Atmos. Chem. Phys., 6, 5037–5048, doi:10.5194/acp-6-5037-2006, 2006.

Giver, L. P., Valero, F. P. J., Goorvitch, D., and Bonomo, F. S.: Nitric-acid band intensities and band-model parameters from 610 to 1760 cm^{-1}, J. Opt. Soc. Am. B, 1, 715–722, 1984.

Goldman, A., Kyle, T. G., and Bonomo, F. S.: Statistical band model parameters and integrated intensities for the 5.9-µm, 7.5-µm, and 11.3-µm bands of HNO_3 vapor, Appl. Optics, 10, 65–73, 1971.

Goldman, A., Rinsland, C. P., Perrin, A., and Flaud, J.-M.: HNO_3 line parameters: 1996 HITRAN update and new results, J. Quant. Spectrosc. Ra., 60, 851–861, 1998.

Gomez, L., Tran, H., Perrin. A., Gamache, R. R., Laraia, A., Orphal, J., Chelin, P., Fellows, C. E., and Hartmann, J. M.: Some improvements of the HNO_3 spectroscopic parameters in the spectral region from 600 to 950 cm^{-1}, J. Quant. Spectrosc. Ra., 110, 675–686, 2009.

Hjorth, J., Ottobrini, G., Cappellani, F., and Restelli, G.: A Fourier transform infrared study of the rate constant of the homogeneous gas-phase reaction $N_2O_5 + H_2O$ and determination of absolute infrared band intensities of N_2O_5 and HNO_3, J. Phys. Chem., 91, 1565–1568, 1987.

Irie, H., Sugita, T., Nakajima, H., Yokota, T., Oelhaf, H., Wetzel, G., Toon, G. C., Sen, B., Santee, M. L., Terao, Y., Saitoh, N., Ejiri, M.K., Tanaka, T., Kondo, Y., Kanzawa, H., Kobayashi, H., and Sasano, Y.: Validation of stratospheric nitric acid profiles observed by Improved Limb Atmospheric Spectrometer (ILAS) – II., J. Geophys. Res., 111, D11S03, doi:10.1029/2005JD006115, 2006.

Jacquinet-Husson, N., Crepeau, L., Armante, R., Boutammine, C., Chédin, A., Scott, N. A., Crevoisier, C., Capelle, V., Boone, C., Poulet-Crovisier, N., Barbe, A., Campargue, A., Benner, D. C., Benilan, Y., Bézard, B., Boudon, V., Brown, L. R., Coudert, L. H., Coustenis, A., Dana, V., Devi, V. M., Fally, S., Fayt, A., Flaud, J.-M., Goldman, A., Herman, M., Harris, G. J., Jacquemart, D., Jolly, A., Kleiner, I., Kleinböhl, A., Kwabia-Tchana, F., Lavrentieva, N., Lacome, N., Li-Hong Xu, Lyulin, O. M., Mandin, J.-Y., Maki, A., Mikhailenko, S., Miller, C. E., Mishina, T., Moazzen-Ahmadi, N., Müller, H. S. P., Nikitin, A., Orphal, J., Perevalov, V., Perrin, A., Petkie, D. T., Predoi-Cross, A., Rinsland, C. P., Remedios, J. J., Rotger, M., Smith, M. A. H., Sung, K., Tashkun, S., Tennyson, J., Toth, R. A., Vandaele, A.-C., and Vander Auwera, J.: The 2009 Edition of the GEISA Spectroscopic Database, J. Quant. Spectrosc. Ra., 112, 2395–2445, 2011.

Kleinert, A., Aubertin, G., Perron, G., Birk, M., Wagner, G., Hase, F., Nett, H., and Poulin, R.: MIPAS Level 1B algorithms overview: operational processing and characterization, Atmos. Chem. Phys., 7, 1395–1406, doi:10.5194/acp-7-1395-2007, 2007.

Laraia, A., Gamache, R. R., Hartmann, J. M., Perrin, A., and Gomez, L.: Theoretical calculations of N_2-broadened halfwidths of ν_5 transitions of HNO_3, J. Quant. Spectrosc. Ra., 110, 687–699, 2009.

Massie, S. T., Goldman, A., Murcray, D. G., and Gille, J. C.: Approximate absorption cross sections of F12, F11, $C1ONO_2$, N_2O_5, HNO_3, CCl_4, CF_4, F21, F113, F114, and HNO_4, Appl. Optics, 24, 3426–3427, 1985.

May, R. D. and Webster, C. R.: Measurements of line positions, intensities, and collisional air broadening coefficients in the HNO_3 7.5 µm band using a computed – controlled tunable diode laser spectrometer, J. Mol. Spectrosc., 138, 383–397, 1989.

Mencaraglia, F., Bianchini, G., Boscaleri, A., Carli, B., Ceccherini, S., Raspollini, P., Perrin. A., and Flaud, J.-M.: Validation of MIPAS satellite measurements of HNO_3 using comparison of rotational and vibrational spectroscopy, J. Geophys. Res., 111, D19305, doi:10.1029/2005JD006099, 2006.

MIPAS-2015 linelist: available at: http://atmos.difa.unibo.it/spectdb/hno3_mipas_2015_4.45.par.zip, last access: 29 April 2016.

Perrin, A.: New analysis of the ν_3 and ν_4 bands of HNO_3 in the 7.6 µm region, J. Phys. Chem. A, 117, 13236–13248, 2013.

Perrin, A., Lado-Bordowski, O., and Valentin, A.: The ν_3 and ν_4 interacting bands of HNO_3 line positions and line intensities, Mol. Phys., 67, 249–270, 1989.

Perrin, A., Flaud, J.-M., Camy-Peyret, C., Jaouen, V., Farrenq, R., Guelachvili, G., Kou, Q., Le Roy, F., Morillon-Chapey, M., Orphal, J., Badaoui, M., Mandin, J.-Y., and Dana, V.: Line intensities in the 11- and 7.6-µm bands on HNO_3, J. Mol. Spectrosc., 160, 524–539, 1993.

Perrin, A., Orphal, J., Flaud, J.-M., Klee, S., Mellau, G., Mäder, H., Walbrodt, D., and Winnewisser, M.: New analysis of the ν_5 and $2\nu_9$ bands of HNO_3 by infrared and millimeter wave techniques: line positions and intensities, J. Mol. Spectrosc., 228, 375–391, 2004.

Raspollini, P., Belotti, C., Burgess, A., Carli, B., Carlotti, M., Ceccherini, S., Dinelli, B. M., Dudhia, A., Flaud, J.-M., Funke, B., Höpfner, M., López-Puertas, M., Payne, V., Piccolo, C., Remedios, J. J., Ridolfi, M., and Spang, R.: MIPAS level 2 operational analysis, Atmos. Chem. Phys., 6, 5605–5630, doi:10.5194/acp-6-5605-2006, 2006.

Raspollini, P., Carli, B., Carlotti, M., Ceccherini, S., Dehn, A., Dinelli, B. M., Dudhia, A., Flaud, J.-M., López-Puertas, M., Niro, F., Remedios, J. J., Ridolfi, M., Sembhi, H., Sgheri, L., and von Clarmann, T.: Ten years of MIPAS measurements with ESA Level 2 processor V6 – Part 1: Retrieval algorithm and diagnostics of the products, Atmos. Meas. Tech., 6, 2419–2439, doi:10.5194/amt-6-2419-2013, 2013.

Remedios, J. J., Leigh, R. J., Waterfall, A. M., Moore, D. P., Sembhi, H., Parkes, I., Greenhough, J., Chipperfield, M. P., and Hauglustaine, D.: MIPAS reference atmospheres and comparisons to V4.61/V4.62 MIPAS level 2 geophysical data sets, Atmos. Chem. Phys. Discuss., 7, 9973–10017, doi:10.5194/acpd-7-9973-2007, 2007.

Ridolfi, M., Carli, B., Carlotti, M., von Clarmann, T., Dinelli, B. M., Dudhia, A., Flaud, J.-M., Hoepfner, M., Morris, P. E., Raspollini, P., Stiller, G., and Wells, R. J.: Optimized forward model and retrieval scheme for MIPAS near-real-time data processing, Appl. Optics, 39, 1323–1340, 2000.

Rotger, M., Boudon, V., and Vander Auwera, J.: Line positions and intensities in the ν_{12} band of ethylene near 1450 cm^{-1}: an experimental and theoretical study, J. Quant. Spectrosc. Ra., 109, 952–962, 2008.

Rothman, L. S., Gordon, I. E., Barbe, A., Chris Benner, D., Bernath, P. F., Birk, M., Boudon, V., Brown, L. R., Campargue, A., Champion, J.-P., Chance, K., Coudert, L. H., Dana, V., Devi, V. M., Fally, S., Flaud, J.-M., Gamache, R. R., Goldman, A., Jacquemart, D., Kleiner, I., Lacome, N., Lafferty, W. J., Mandin, J.-Y., Massie, S. T., Mikhailenko, S. N., Miller, C. E., Moazzen-Ahmadi, N., Naumenko, O. V., Nikitin, A. V., Orphal, J., Perevalov, V. I., Perrin, A., Predoi-Cross, A., Rinsland, C. P., Rotger, M., Simeckova, M., Smith, M. A. H., Sung, K., Tashkun, S. A., Tennyson, J., Toth, R. A., Vandaele, A. C., and Vander Auwera, J.: The HITRAN 2008 molecular spectroscopic database, J. Quant. Spectrosc. Ra., 110, 533–572, 2009.

Rothman, L. S., Gordon, I. E., Babikov, Y., Barbe, A., Chris Benner, D., Bernath, P. F., Birk, M., Bizzocchi, L., Boudon, V., Brown, L. R., Campargue, A., Chance, K., Cohen, E. A., Coudert, L. H., Devi, V. M., Drouin, B. J., Fayt, A., Flaud, J.-M., Gamache, R. R., Harrison, J. J., Hartmann, J.-M., Hill, C., Hodges, J. T., Jacquemart, D., Jolly, A., Lamouroux, J., Le Roy, R. J., Li, G., Long, D. A., Lyulin, O. M., Mackie, C. J., Massie, S. T., Mikhailenko, S., Müller, H. S. P., Naumenko, O. V., Nikitin, A. V., Orphal, J., Perevalov, V., Perrin, A., Polovtseva, E. R., Richard, C., Smith, M. A. H., Starikova, E., Sung, K., Tashkun, S., Tennyson, J., Toon, G. C., Tyuterev, V. I. G., and Wagner, G.: The HITRAN2012 Molecular Spectroscopic Database, J. Quant. Spectrosc. Ra., 130, 4–50, 2013.

Sharpe, S. W., Johnson, T. J., Sams, R. L., Chu, P. M., Rhoderick, G. C., and Johnson, P. A.: Gas-phase databases for quantitative infrared spectroscopy, Appl. Spectrosc., 58, 1452–1465, 2004.

Tran, H., Brizzi, G., Gomez, L., Perrin, A., Hase, F., Ridolfi, M., and Hartmann, J. M.: Validation of HNO_3 spectroscopic parameters using atmospheric absorption and emission measurements, J. Quant. Spectrosc. Ra., 110, 109–117, 2009.

Wang, D. Y., Höpfner, M., Blom, C. E., Ward, W. E., Fischer, H., Blumenstock, T., Hase, F., Keim, C., Liu, G. Y., Mikuteit, S., Oelhaf, H., Wetzel, G., Cortesi, U., Mencaraglia, F., Bianchini, G., Redaelli, G., Pirre, M., Catoire, V., Huret, N., Vigouroux, C., De Mazière, M., Mahieu, E., Demoulin, P., Wood, S., Smale, D., Jones, N., Nakajima, H., Sugita, T., Urban, J., Murtagh, D., Boone, C. D., Bernath, P. F., Walker, K. A., Kuttippurath, J., Kleinböhl, A., Toon, G., and Piccolo, C.: Validation of MIPAS HNO_3 operational data, Atmos. Chem. Phys., 7, 4905–4934, doi:10.5194/acp-7-4905-2007, 2007.

Wespes, C., Hurtmans, D., Clerbaux, C., Santee, M. L., Martin, R. V., and Coheur, P. F.: Global distributions of nitric acid from IASI/MetOP measurements, Atmos. Chem. Phys., 9, 7949–7962, doi:10.5194/acp-9-7949-2009, 2009.

Wolff, M. A., Kerzenmacher, T., Strong, K., Walker, K. A., Toohey, M., Dupuy, E., Bernath, P. F., Boone, C. D., Brohede, S., Catoire, V., von Clarmann, T., Coffey, M., Daffer, W. H., De Mazière, M., Duchatelet, P., Glatthor, N., Griffith, D. W. T., Hannigan, J., Hase, F., Höpfner, M., Huret, N., Jones, N., Jucks, K., Kagawa, A., Kasai, Y., Kramer, I., Küllmann, H., Kuttippurath, J., Mahieu, E., Manney, G., McElroy, C. T., McLinden, C., Mébarki, Y., Mikuteit, S., Murtagh, D., Piccolo, C., Raspollini, P., Ridolfi, M., Ruhnke, R., Santee, M., Senten, C., Smale, D., Tétard, C., Urban, J., and Wood, S.: Validation of HNO_3, $ClONO_2$, and N_2O_5 from the Atmospheric Chemistry Experiment Fourier Transform Spectrometer (ACE-FTS), Atmos. Chem. Phys., 8, 3529–3562, doi:10.5194/acp-8-3529-2008, 2008.